Kinetics of viral load, immunological mediators and characterization of a SARS-CoV-2 isolate in mild COVID-19 patients during acute phase of infection

Running Title: Virus and inflammation in mild COVID-19 cases

Anbalagan Anantharaj[1*], Sunil Gujjar[1*], Saurabh Kumar[1*], Nikhil Jain[2], Jigme Wangchuk[1], Naseem Ahmed Khan[1], Aleksha Panwar[1], Akshay Kanakan[3], Vivekanand A[3,4], Janani Srinivasa Vasudevan[3], Asim Das[2], Anil Kumar Pandey[2], Rajesh Pandey[3] and Guruprasad R. Medigeshi[1]

1: Clinical and Cellular Virology lab and Bioassay Laboratory, Translational Health Science and Technology Institute, Faridabad, Haryana. INDIA.

2: Employees State Insurance Corporation Medical College and Hospital, Faridabad, Haryana, INDIA.

3: CSIR-Institute of Genomics and Integrative Biology, Delhi, INDIA.

4: Academy of Scientific and Innovative Research (AcSIR), Ghaziabad-201002, INDIA.

* These authors contributed equally

 # Corresponding author:

Guruprasad R. Medigeshi, PhD

Translational Health Science and Technology Institute,

NCR-Biotech Science Cluster,

P.O. Box # 4, Faridabad-Gurgaon Highway,

Faridabad 121001. INDIA.

Tel: +91-0129-2876311.

Email: gmedigeshi@thsti.res.in

ABSTRACT

Over 95% of the COVID-19 cases are mild-to-asymptomatic who contribute to disease transmission whereas most of the severe manifestations of the disease are observed in elderly and in patients with comorbidities and dysregulation of immune response has been implicated in severe clinical outcomes. However, it is unclear whether asymptomatic or mild infections are due to low viral load or lack of inflammation. We have measured the kinetics of SARS-CoV-2 viral load in the respiratory samples and serum markers of inflammation in hospitalized COVID-19 patients with mild symptoms. We observed a bi-phasic pattern of virus load which was eventually cleared in most patients at the time of discharge. Viral load in saliva samples from a subset of patients showed good correlation with nasopharyngeal samples. Serum interferon levels were downregulated during early stages of infection but peaked at later stages correlating with elevated levels of T-cell cytokines and other inflammatory mediators such as IL-6 and TNF- α which showed a bi-phasic pattern. The clinical recovery of patients correlated with decrease in viral load and increase in interferons and other cytokines which indicates an effective innate and adaptive immune function in mild infections. We further characterized one of the SARS-CoV-2 isolate by plaque purification and show that infection of lung epithelial cells (Calu-3) with this isolate led to cytopathic effect disrupting epithelial barrier function and tight junctions. Finally we showed that zinc was capable of inhibiting SARS-CoV-2 infection in this model suggesting a beneficial effect of zinc supplementation in COVID-19 infection.

IMPORTANCE

A majority of COVID-19 patients are asymptomatic or exhibit mild symptoms despite high viral loads suggesting a key role for the acute phase innate immune response in limiting the damage

and clearing the virus. Therefore, it is important to understand the early phase response to SARS-CoV-2 infection in such patients to devise strategies for clinical management of the disease. Our study shows the kinetics of immune mediators in the serum samples collected from hospitalized COVID-19 patients with mild symptoms. We further characterize a virus isolate from one of these patients and demonstrate its effect on epithelial barrier functions and show that zinc was capable of inhibiting SARS-CoV-2 infection under these conditions. Our results suggest a key role for the innate immune responses in the early phase of infection in mitigating clinical symptoms, clearing the virus and recovery from illness and suggest an antiviral role for zinc in COVID-19 infection.

Keywords: SARS-CoV-2; COVID-19; Cytokines; Chemokines; Inflammation; Zinc; epithelial cells.

60 **INTRODUCTION**

61 Coronavirus disease of 2019 (COVID-19) has infected over 35 million people worldwide leading
62 to over a million deaths (as on 10th October 2020). Severe acute respiratory syndrome
63 coronavirus-2 (SARS-CoV-2), a positive-sense RNA virus from the family *Coronaviridae* is the
64 causative agent of COVID-19. The RNA genome of SARS-CoV-2 ranges from 26 to 32
65 kilobases in length and similar to other coronaviruses that have jumped species to infect humans,
66 SARS-CoV-2 is believed to have been in circulation in animals such as bats for several decades
67 before infecting humans (1). The genome of SARS-CoV-2 shares about 96% identity with that of
68 bat coronavirus and is about 80% identical to the SARS-CoV-1 (2). Angiotensin converting
69 enzyme-2 (ACE2) has been reported as a primary entry receptor for SARS-CoV-2 (3). ACE2, a
70 type I membrane protein, is expressed in lungs, kidneys, intestine and heart. The spike
71 glycoprotein (S-protein) on the SARS-CoV-2 virion surface mediates the receptor recognition
72 and membrane fusion thus facilitating the entry of virus in the cell (4). There are close to 200
73 vaccines under development for COVID-19 and some of the vaccines have advanced to Phase III
74 trials (5). Efforts to repurpose drugs and to manage the cytokine storm have identified a number
75 of drugs that have been recommended for use in COVID-19 (6) but an effective antiviral specific
76 to SARS-CoV-2 is yet to be licensed for human use.

77

78 Most of the patients with COVID-19 exhibit mild or no symptoms and severe clinical symptoms
79 are observed in patients in the older age group (>65 years) or patients with underlying
80 comorbidities such as hypertension and diabetes. Impaired immune response and cytokine storm
81 has been implicated in clinical manifestations observed in severe disease (7-9). Increased viral
82 load has been shown to correlate with disease severity (7, 10) and some of the antivirals such as

83 Remdesivir which inhibit the viral RNA-dependent-RNA-polymerase of SARS-CoV-1, Middle
84 East Respiratory Syndrome Coronavirus (MERS-CoV) and SARS-CoV-2 has been shown to
85 reduce time to recovery and mortality in COVID-19 patients (11). As is the case with RNA
86 viruses, coronaviruses accumulate mutations and evolve at a rate similar to other RNA viruses
87 (12, 13). Variations in the viral genome and emergence of novel clades has been implicated in
88 increased fitness and transmission (14) however there is no evidence to suggest increased
89 virulence of infecting virus as a cause of severe disease in COVID-19 patients suggesting that
90 the host response and underlying comorbidities plays a key role in clinical outcomes (15). In this
91 study, we monitored the kinetics of viral load in respiratory samples and saliva and cytokines and
92 chemokines in the serum of hospitalized COVID-19 patients who displayed mild/moderate
93 symptoms and recovered from illness. We isolated SARS-CoV-2 from one of the patients and
94 further characterized the isolate by plaque-purification and sequencing and assessed the effect of
95 virus infection on epithelial barrier functions. Our results suggest a clear inverse correlation
96 between interferon response and viral load and identifies signatures in the inflammatory
97 mediators in the serum of young patients who recover from COVID-19. We also show that the
98 virus isolate from a patient with mild infection is capable of infecting lung epithelial cells and
99 disrupting epithelial barrier functions leading to cell death further underscoring the importance of
100 a robust host response in mitigating the clinical outcomes in COVID-19 infection. Finally,
101 addition of zinc post-infection inhibited SARS-CoV-2 infection indicating the antiviral function
102 of zinc in SARS-CoV-2 life-cycle.
103
104 **MATERIALS AND METHODS**
105

106 **Human Ethics**

107 The study was approved by the Institutional ethics committees for human research at both the
108 institutions (No. 134/A/11/16/Academics/MC/2016/134 and THS 1.8.1/ (93)). Informed consent
109 was obtained from all the participants.

110

111 **Clinical samples**

112 Patients with symptoms of COVID-19 infection were diagnosed using RealStar® SARS-CoV-2
113 RT-PCR kit (altona Diagnostics GmbH) at ESIC Medical College & Hospital. Clinical
114 presentations were mild or asymptomatic (identified by contact tracing) and included mild to
115 moderate fever, dry cough, and loss of sense of smell and taste. As per the regulations at the time
116 of the study, all patients with a positive RT-PCR test were admitted to the hospital within 24-48
117 hours of testing positive and treated with azithromycin with hydroxychloroqine, Vitamin C and
118 D. Samples were collected from patients who consented to participate in the study by signing the
119 informed consent form. Nasopharyngeal/oropharyngeal (NP/OP) swab in virus transport medium
120 (VTM), saliva and serum was collected from Day 1 of enrolment till discharge. Saliva was
121 collected in specimen collection cups early in the morning immediately after the patient woke up
122 from sleep. All the samples collected daily at same interval. All patients were isolated in the
123 hospital for at least 14 days.

124

125 **Virus culture and isolation**

126 SARS-CoV-2 Isolate USA-WA1/2020 was obtained from BEI resources (deposited by the
127 Centers for Disease Control and Prevention and obtained through BEI Resources, NIAID, NIH:
128 SARS-Related Coronavirus 2, Isolate USA-WA1/2020, NR-52281). Indian isolates of SARS-

129 CoV-2 was isolated from COVID-19-positive VTM samples (VTM) using Vero E6 cells
130 (Obtained from National Centre for Cell Science, Pune, INDIA). $2x10^6$ cells were grown in a
131 T25 flask to about 80% confluency. Culture medium was removed and washed once with 5 ml of
132 phosphate-buffered saline (PBS). 500 µl of VTM was added onto the cells and the flask was
133 incubated for 1 h at 37ºC in a CO_2 incubator with intermittent mixing. After 1h of adsorption,
134 monolayer was washed twice with 1X PBS and DMEM supplemented with 2% fetal bovine
135 serum (FBS) and 2X antibiotics (200 units of penicillin, 200 µg of streptomycin) and 250 ng/ml
136 amphotericin B and non-essential amino acids. Cell monolayer was observed under the
137 microscope every day. Cytopathic effect was observed usually by day two of infection when the
138 Ct value of the sample was less than 20 in RT-PCR. Culture supernatant was harvested and
139 clarified at 1000 x *g* and multiple small aliquots were prepared and stored at -80ºC.Virus titer in
140 the supernatants were estimated by plaque assays on Vero E6 cells as per the previous protocols
141 (16) except that the cells were fixed at 60 h pi. Clinical specimens and virus cultures were
142 handled in biosafety level 3 (BSL3) facility as per the standard operating procedure and
143 guidelines for BSL3 level pathogen.
144
145 **Quantitative RT PCR**
146 RNA was extracted from 150 µl of VTM using Viral RNA Isolation Kit (MACHEREY-
147 NAGEL), and eluted in 50 µl of nuclease-free water and used as a template for quantitation of
148 SARS-CoV-2 viral RNA levels by reverse transcription polymerase chain reaction (RT-PCR).
149 2019-nCoV CDC Probe and Primer kit for SARS-CoV-2 manufactured (Biosearch
150 Technologies) was used to detect N gene by real time RT PCR. RNAse P was detected as
151 endogenous control for normalization. The region of N gene starting from 28287 – 29230 was

152 amplified using the forward primer 5'-GACCCCAAAATCAGCGAAAT-3' and the reverse
153 primer 5'-GCGCGACATTCCGAAGAA-3' and cloned into pGEM®-T-Easy vector (Promega).
154 This clone was linearized using Sac II enzyme and *in vitro* transcribed using the SP6 RNA
155 polymerase (Promega). The transcript was purified and used as a template for generating
156 standard curve to estimate the copy number.

157 For virus isolates, RNA was isolated from 4 different plaque-purified isolates using
158 QIAamp Viral RNA mini kit (Qiagen) according to manufactures instruction. SARS-CoV-2 viral
159 RNA was detected using RealStar® SARS-CoV-2 RT-PCR kit (altona Diagnostics GmbH). To
160 check the presence of other respiratory virus in samples, FTlyo respiratory pathogen 21 plus kit
161 was used (Fast Track Diagnostics). This detects presence of 21 respiratory viruses which
162 includes influenza A virus; influenza A(H1N1) virus (swine-lineage); influenza B virus; human rhinovirus;
163 human coronaviruses NL63, 229E, OC43 and HKU1; human parainfluenza viruses 1, 2, 3 and 4; human
164 metapneumoviruses A/B; human bocavirus; human respiratory syncytial viruses A/B; human adenovirus;
165 enterovirus; human parechovirus; *Mycoplasma pneumoniae* and 4 bacterial species *S. aureus*; *C.*
166 *pneumoniae*; *H. influenzae* B; *S. pneumonia.*

167

168 **Multiplex cytokine/chemokine assays**

169 25 µl of serum was used for in magnetic bead-based multiplex chemokine and cytokine luminex
170 assay as per the manufacturer's instructions (Merck-Millipore). Assays were performed in
171 duplicates along with quality controls. The amount of each analyte was estimated by standard
172 curve generated using known amount of analyte provided in the assay kit. Assay plates were read
173 using MAGPIX system and data was analysed by xPONENT software using five parametric
174 logistic fit model.

175

176 **Cell Viability assay**

177 Cell viability assay was performed using CellTiter-Glo® Assay kit (Promega) according to user
178 manual. Briefly, 20,000 Calu-3 cells were seeded in 96 well plate and grown for 48 h. Cells were
179 treated with zinc sulfate at indicated concentrations. After 24 h post treatment CellTiter-Glo
180 reagent was added to the well and luminescence was measured by microplate reader (Synergy
181 HT - BioTek).

182

183 **Labile zinc level measurement**

184 Labile Zn levels in the cells were estimated as described before (17). Briefly, after incubation
185 with zinc sulfate, cells were washed once with PBS, detached using trypsin and resuspended in
186 staining medium (DMEM without phenol red supplemented and with 2 mM L-glutamine; Gibco)
187 containing 2.5 µM ZinPyr-1 (ZP-1) (Santa Cruz) for 30 min at 37°C. Cells were washed using
188 fluorescence-activated cell sorter (FACS) buffer (PBS containing 0.25% FBS), and samples were
189 acquired in a FACS Canto II apparatus (Becton, Dickinson). The amounts of labile zinc present
190 in the cells are presented as the mean fluorescence intensities of ZP-1.

191

192 **Immunofluoresence**

193 VeroE6, Calu-3 (ATCC) and Caco-2 (ATCC) cells were seeded at 50,000 cells per well in 48-
194 well plate. Calu-3 and Caco-2 cells were seeded 2 days prior whereas VeroE6 were seeded a day
195 before infection. Cells were infected with SARS-CoV-2 THSTI-BL2010-D at 0.3, 1 and 3 MOI.
196 After 1 h of adsorption, viral inoculum was removed. Cells were washed twice with PBS. Cells
197 were kept in complete medium (10% FBS containing DMEM with penicillin, streptomycin and

198 glutamine mix and non-essential amino acids). At 24 h pi, cells were washed twice with PBS and
199 once with cold PBS and fixed by using ice cold methanol and kept at -20ºC for 20 min. Methanol
200 was removed, cells were washed once with cold PBS and then once with PBS at room
201 temperature (RT), followed by blocking with 0.2% BSA-PBS for 10 min at RT. Cells were
202 incubated with human chimeric SARS-CoV-2 S1 spike antibody (1: 100 dilution; Genescript –
203 HC2001) in 0.2% BSA-PBS for 1h at RT. Cells were then washed three times with 0.2% BSA-
204 PBS. This was followed by incubation with secondary antibody conjugated with anti-human
205 Alexa flour 488 (1:500; Life Technologies–A11013) for 30 min at room temperature in dark.
206 Cells were washed with PBS three times and stained with 4′,6-diamidino-2-phenylindole (DAPI)
207 (Molecular probes) at 1:10,000 dilution for 10 min. Cells were washed with PBS and images
208 were captured using Olympus DP80 microscope at 20X magnification. Images were processed
209 by background subtraction using cellSens software. Bright field images were captured using
210 Nikon Eclipse Ti-S at 10X magnification.
211
212 **Zinc treatment**
213 Calu-3 cells (40-50K) were seeded in a 24-well plate and two days post-infection, cells were
214 infected with 0.3 MOI of SARS-CoV-2. Cells were cultured in serum-free MEM containing
215 indicated concentrations of zinc sulfate for 24 hours. Viral titers in the supernatant was measured
216 by plaque assays as described above.
217
218 **Whole genome Sequencing and analysis**
219 The protocol followed for the sample preparation, sequencing, and data analysis has been
220 described earlier (18). In brief, double-stranded cDNA was synthesized from 50ng of total RNA

221 from virus stocks for all the four plaque-purified SARS-CoV-2 isolates. The first strand of
222 cDNA was synthesized using Superscript IV followed by RNA digestion with RNase H for
223 second-strand synthesis using DNA Polymerase I Large fragment (Klenow fragment). 100ng of
224 purified double-stranded cDNA was taken for forward using ARTIC tiling PCRprotocol (V3
225 primer pools) (https://artic.network/ncov-2019) (19). 200ng of each purified sample of
226 multiplexed PCR amplicons obtained was taken for library preparation using Oxford Nanopore
227 Technology (ONT). This included End Repair/dA tailing, Native Barcode Ligation, and Adapter
228 Ligation of the PCR amplicons. 100ng of the pooled and purified library was sequenced using
229 ONT's MinION Mk1B platform (18).
230 Samples were base-called and demultiplexed using Guppy basecaller (version
231 3.5.2)(https://community.nanoporetech.com). Reads having phred quality score < 7 were
232 discarded to filter the low-quality reads. The resulting fastq files were normalized by read length
233 (300-500) and reads were aligned using Minimap2 (v2.17) (20) to the reference (GenBank:
234 MN908947.3). Variants were called using Nanopolish(21)from the aligned reads and further
235 creating consensus fasta using bcftools (v1.8). Finally, we used Nextclade
236 (https://clades.nextstrain.org/) for the detection of clades from the consensus fastasequence.All
237 the sequences are submitted to the GISAID database (https://www.gisaid.org/ ; GISAID EPI ISL
238 - 454862).
239
240 **Phylogenetic analysis**
241 The consensus genomes obtained from the whole genome sequencing of 10 Indian isolates and
242 four plaque-purified Indian isolates along with 86 other global SARS-CoV-2 sequences were
243 used for constructing the phylogeny. The sequences were selected from a diverse geographical

244 location to represent the global distribution and spread of the virus. The sequences were obtained
245 from the Global Initiative on Sharing All Influenza Data (GISAID) database. The fasta
246 sequences were aligned using MUSCLE (22). A maximum-likehood Phylogeny was generated
247 using FastTree 2.1.11 (23)with generalized time-reversible (GTR) substitution model and 1000
248 bootstrap replicates with default parameters. The tree was visualized and edited using ITOL (24).
249

250 **Trans-epithelial electrical resistance and confocal microscopy**

251 Calu-3 cells were grown in air-liquid interface as described elsewhere (25). Briefly, Calu-3 cells
252 were seeded at 30,000 on 3 µm pore size transwell inserts (Corning - 3415). Cells were
253 maintained at liquid-liquid interface for 7 days and cells were further grown with 600 µl of
254 complete medium only in the basolateral compartment. Media was replaced every alternate day.
255 TEER was monitored at indicated time points using a chop stick electrode (Millipore). On day 21
256 post-seeding, cells were infected with SARS-CoV-2-THSTI-BL2010D as described. At 24 h
257 pi, culture inserts were washed with cold 1X PBS and incubated with cold methanol at −20°C for
258 20 minutes. Cells were further incubated with IMF buffer (20 mM HEPES, pH 7.5, 0.1% Triton-
259 X-100, 150 mM sodium chloride, 5 mM EDTA and 0.02% sodium azide as a preservative) for 5
260 min at room temperature (RT) and all further washes were performed with IMF buffer. Non-
261 specific antibody binding sites were blocked by incubating cells with IMF buffer containing 2%
262 normal goat serum for 10 min at RT. Membranes were cut out using a scalpel blade and
263 transferred to a 48-well plate. Cells were washed three times followed by incubation with
264 antibodies against ZO-1 (Becton Dickinson), Claudin-3 (Invitrogen), SARS-CoV-2 spike
265 antibody in IMF buffer (20 mM HEPES pH 7.5, 0.1% Triton X-100, 150 mM NaCl, 5 mM
266 EDTA, 0.02 % sodium azide) for 1 h at RT. Cells were washed followed by incubation with

267 appropriate secondary antibodies tagged with Alexa fluor 488/568/633 (Molecular probes) for 30
268 min at RT by avoiding exposure to light. Cells were washed with IMF buffer three times and
269 stained with DAPI at 1:10,000 dilution for 10 min. Cells were washed with PBS, mounted on
270 glass slide using antifade solution (Molecular probes) and images were captured at 100X
271 magnification using FV3000 confocal microscope (Olympus). Images were processed by
272 background subtraction using cellSens software (Olympus).
273

274 **Data analysis**

275 Data was analysed and final graphs were prepared using GraphPad Prism (Version 7.0e)
276 software. All experiments were performed with two or more replicates and graphs have been
277 prepared representing data from at least two independent experiments with $n \geq 6$ unless
278 otherwise indicated. Statistical significance was estimated by t-test (unpaired, non-parametric)
279 using Mann-Whitney method.
280

281 **RESULTS**

282 **Kinetics of viral load in COVID-19 patients with mild symptoms**

283 11 patients who were positive for COVID-19 by RT-PCR were enrolled for the study after
284 obtained informed consent. The median age of the patients was 32 (25% Percentile 24, 75%
285 Percentile 45) and the mean duration of hospitalization was 14 days (Std. Dev. 4.034 days). Out
286 of the 11 patients 6 were male and 5 were female. NP & OP swabs, saliva and serum samples
287 collected for a maximum of 10 days. Most of the patients in this study manifested mild
288 symptoms and were asymptomatic at the time of discharge. We measured daily viral load in the
289 NP/OP samples by RT-PCR. For a subset of patients (n=5), we collected saliva samples early in

290 the morning for estimation of viral load in saliva and compare with the NP/OP sample. Viral
291 load in NP/OP swab samples peaked between day 2 to 4 in most patients and we observed a
292 biphasic increase in viral RNA levels in few patients with a second peak on day 5 (Figure 1A-
293 1F). The peak viral RNA levels ranged from 10^6 to 10^{10} copies per ml of virus transport medium.
294 Except for one patient, viral load in saliva correlated with viral load in VTM samples (Figure
295 1H-1K). In one patient, virus persisted in saliva till day 10 while the VTM sample was RT-PCR
296 negative by day 6 of enrolment (Figure 1G). In most cases, the viral RNA was below the level
297 of detection by RT-PCR by day 7-9 but two patients showed increasing trend in viral RNA levels
298 although the last sample in these patients were on day 5 and day 7 (Figure 1D and 1H). These
299 data suggest that the mild or asymptomatic patients harbour high viral load and salivary viral
300 load can be a good alternate for the NP/OP swabs.
301

302 **Kinetics of inflammatory mediators in mild/asymptomatic COVID-19 patients**

303 As recent reports implicate both virus and host factors in severe COVID-19 disease, we were
304 interested in estimating the levels of some of the inflammatory mediators along with interferons
305 in the serum samples collected daily from mild COVID-19 patients to understand the correlates
306 of recovery from disease. We measured 15 serum inflammatory mediators in each of the samples
307 by multiplexing using luminex technology. The analytes detected are namely IFN-α2, IFN-γ, IL-
308 1β, IL-4, IL6, IL-7, IL-8, IL10, IL12p40, IL12p70, IL17A, Monocyte Chemotactic Protein
309 1(MCP-1), MCP-3, TNF-α and gamma interferon inducible protein -10 (IP-10). We observed a
310 consistent decrease in type I and type II during the acute phase of infection but both IFN-α2 and
311 IFN-γ increased at later stages of infection coinciding with recovery and clearance of virus by
312 day 8 of enrolment (Figure 2A). We next looked at the cytokines that influence T-cell functions

313 namely the pro-inflammatory IL-12p40 homodimer or IL-12p70, the active IL-12 heterodimer
314 secreted by dendritic cells and macrophages that promotes Th1 response and leads to IFN-γ and
315 TNF-α production. We observed a clear increase in IL-12p70 levels from day 5 onwards
316 suggesting priming of T cells by the innate immune system through IL-12p70 secretion (Figure
317 2B). This increase coincided with increased IFN-γ levels observed in the same samples (Figure
318 1A). IL-7, a cytokine produced by epithelial cells and DCs and promotes biogenesis and
319 proliferation of lymphocytes also showed an increasing trend coinciding with IL-12p70.
320 However IL-17A levels did not show a significant change suggesting a more prominent role for
321 Th1 responses in recovery in mild COVID-19 cases. Contrasting with the IFN responses, the
322 levels of IL-8 was elevated at early stages of infection suggesting a key role for innate immune
323 cells such as macrophages which produce IL-8 thus promoting neutrophil recruitment to the site
324 of infection leading to resolution of infection. Interestingly, the levels of other two pro-
325 inflammatory chemokines IP-10 and MCP-1 did not show any variation and MCP-3 levels were
326 very heterogenous during the course of infection in any of the patients suggesting lack of severe
327 inflammatory response in these patients (Figure 2C). IL-6, an acute phase reactant which is
328 implicated in the severe manifestations of severe COVID-19 symptoms showed a moderate
329 increase in multiple phases but TNF-α levels were unchanged in majority of the patients. The
330 levels of IL-10, IL-4 and IL-1β showed an increasing trend in samples from day 5 - day 8 of
331 infection suggesting the activation of T cells (Figure 2D). Overall our data suggests a prominent
332 role for the innate immune response in clearance of virus infection/infected cells at early states of
333 infection and priming of adaptive immune responses which probably lead to long-term protection
334 from re-infection.
335

336 **Isolation and characterization of SARS-CoV-2**

337 Increased viral loads have been associated with severe disease by previous reports (7, 15). We
338 were interested in understanding whether the virus isolates from mild or asymptomatic infection
339 have altered ability to evade immune response and cause cellular damage. In order to isolate and
340 characterize an Indian isolate of SARS-CoV-2, we used NP/OP swab samples from six COVID-
341 19 patients whose samples had a Ct value of 20 or less by the diagnostic RT-PCR. Vero E6 cells
342 were inoculated with NP/OP swab samples and culture supernatant was harvested on day 2 post-
343 infection when cytopathic effect was evident to generate passage 1 virus. The process was
344 repeated two more times to generate passage 2 and passage 3 viruses (Supplementary Figure S1).
345 One of the passage 3 isolate, THSTI-BL2010-D, was further plaque-purified by isolating four
346 individual plaques (THSTI-BL2010-A through D) and propagating further one more time in
347 Vero E6 cells to generate a large stock of passage 5 virus for all experiments (Figure 3A). All the
348 plaque-purified virus showed CPE at 72 h pi. All the plaque-purified viruses were negative for
349 21 respiratory viruses and 4 bacterial species including Mycoplasma as assessed by RT-PCR
350 indicating lack of any secondary pathogens. Next, we performed plaque assays to compare the
351 plaque morphology of plaque-purified virus on VeroE6 cell-monolayer with SARS-CoV-2 USA-
352 WA1/2020 isolate.Both the isolates developed plaques at 60 h pi, however, the plaque-purified
353 isolate produced a more homogenous plaque size and distribution as compared to the USA-
354 WA1/2020 isolate (Figure 3B).

355

356 **SARS-CoV-2 infection in human epithelial cell lines**

357 Infection of SARS-CoV-2 in human cell lines depends on the expression of its receptor
358 angiotensin-converting enzyme 2 (ACE2) and the host protease TMPRSS2 (26). To confirm the

359 infectivity of THSTI-BL2010-D in human cell lines, we infected Vero E6, Calu-3 and Caco-2
360 cells with increasing MOIs of the virus and stained for the presence of spike protein by
361 immunofluorescence assay at 24 h pi. As expected, Vero E6 cells showed the maximum
362 infection followed by Calu-3 cells and Caco-2 cells (Figure 4A). We next compared growth
363 curve of SARS-CoV-2 Wuhan strain and THSTI-BL2010D in Vero E6 cells. Cells were infected
364 with 0.1 MOI of both strains and supernatants were collected at 24, 48 and 72 h pi. Plaque assay
365 results showed titres of Wuhan strain was a log higher than THSTI-BL2010D at 24 h pi whereas
366 at 48 h pi virus titres with both strains were similar (Figure 4B). Virus titers showed a declining
367 trend at 72 h pi most probably due to cytopathic effect.
368
369 **Whole genome sequencing**
370 To further characterize the plaque-purified isolates at molecular level, we isolated RNA from the
371 plaque-purified virus stocks and subjected to whole genome sequencing. All the four plaque-
372 purified virus RNA samples showed similar changes in the nucleotide positions with most
373 changes in the ORF1a region leading to five non-synonymous and one synonymous change in
374 the protein sequence (Table 1). THSTI-BL-2010-C sample had one additional mutation
375 G27806T resulting in a synonymous change in ORF7b. Two non-synonymous changes were also
376 observed in ORF1b and N regions (Table 1). Interestingly, none of the Indian isolates in our
377 study showed D614G mutations observed elsewhere which is associated with increased
378 infectivity (27).The slippery heptanucleotide sequence and the pseudoknot structure were not
379 disrupted in any of the samples as per the sequence alignment compared to the reference genome
380 (Accession ID: MN908947.3). The phylogenetic analysis of the 100 representative SARS-CoV-2
381 sequences from around the world (Supplementary Table S1) revealed clustering of sequences

382 into five major clades according to the GISAID nomenclature system (https://www.gisaid.org).
383 Sequences from all the 14 genomes from our study were subjected to phylogenetic analysis and
384 were assigned to clade 19A which along with the 19B clade forms the earliest clade which
385 originated from Wuhan and was prevalent in Asia during the initial months of the outbreak
386 (Figure 5). This suggests that the SARS-CoV-2 isolates reported in our study are genetically
387 more similar to the reference Wuhan sequence (GenBank: MN908947.3).
388

389 **SARS-CoV-2 infection disrupts epithelial barrier**

390 We were further interested to investigate the effect of THSTI-BL-2010D isolate infection on
391 epithelial barrier functions. Polarized Calu-3 cells grown on transwells were infected with
392 SARS-CoV-2 at 0.3 MOI. TEER was measured at 24 h pi and virus titers in the apical and
393 basolateral supernatants were estimated by plaque assays. We observed a 60% reduction in
394 TEER values as compared to mock at 24 h pi indicating disruption of epithelial barriers as a
395 result of cytopathic effect (Figure 6A). As expected, virus was present both in the apical and
396 basolateral samples due to disruption of cellular junctions and polarity (Figure 6B). Cells were
397 stained for virus spike protein, ZO-1 and claudin-3 antibodies to visualize infected cells and
398 staining pattern of these representative junctional proteins. We observed disruption of both ZO-1
399 and claudin-3 staining in virus-infected cells but not in mock-infected cells (Figure 6C)
400 suggesting that SARS-CoV-2 isolated from an mild/asymptomatic patient infects polarized lung
401 epithelial cells and causes damage to epithelial barriers due to cytopathic effect.
402

403 **Zinc supplementation affects SARS-CoV-2 infection *in vitro***

404 Addition of zinc along with the zinc ionophore pyrithione, which stimulates zinc uptake, was
405 shown to inhibit SARS-CoV infection in Vero E6 cells (28). We were interested to use our cell
406 culture system to assess whether zinc has an inhibitory effect on SARS-CoV-2 infection. We
407 first determined cytotoxicity and uptake of zinc in Calu-3 cells by treating cells with different
408 concentration of $ZnSO_4$ at 25, 50 and 100 μM for 24 h. We observed cytotoxicity beyond 50 μM
409 $ZnSO_4$ in Calu-3 cells (Figure 6D). Zinc uptake was determined by staining cells with zinc
410 fluorophore, ZP-1, at 4 h post-treatment. Cells treated with 25 μM of $ZnSO_4$ showed 25%
411 increase in labile zinc levels whereas cells treated with 50 μM of $ZnSO_4$ shows 50% increase in
412 labile zinc levels as compared to mock-treated control suggesting that these cells are capable of
413 zinc uptake (Supplementary Figure S2). Cells were infected with SARS-CoV-2 at 0.3 MOI and
414 cultured in the presence of 25 and 50 μM of $ZnSO_4$ for 24 h. At 24 h pi viral titres in the
415 supernatant was determined by plaque assay. Zinc treatment showed over three-fold reduction in
416 viral titers at 24 h pi as compared to untreated cells (Figure 6E) indicating the antiviral effect of
417 zinc salts on SARS-CoV-2 infection in these cells.
418

419 **Discussion**

420 Of all the coronavirus epidemic/pandemic of recent past, COVID-19 has had the maximum
421 impact on global health and economy. Although most of the individuals are asymptomatic or
422 with mild symptoms, the disease affects the elderly and people with co-morbidities the most
423 indicating a critical role for innate immune response in limiting the viral load and spread. Most
424 asymptomatic or individuals with mild symptoms harbour high viral loads in their respiratory
425 tract and contribute to disease transmission. Previous report suggested reduced interferon
426 response in severe patients as compared to mild/moderate cases 8-12 days after the onset of

427 symptoms (7) and viral genetics was not found to correlate with severe disease (15). We
428 focussed our efforts to monitor the kinetics of viral load and inflammatory mediators in the
429 serum samples of hospitalized COVID-19 patients who displayed mild to no symptoms but were
430 RT-PCR positive for SARS-CoV-2 during screening at the hospital or contact tracing. Most of
431 our patients were enrolled within 48 hours of testing positive and are likely to be within the first
432 week of exposure to the virus. In patients where we could detect viral RNA in saliva samples, the
433 viral load in saliva correlated well with the same in VTM samples suggesting that saliva sample
434 could replace NP/OP swabs which cause discomfort to patients during sample collection.
435 Collection of saliva would also reduce the cost and time involved in sample collection for
436 COVID-19 diagnosis and self-sampling by patients would reduce the risk of exposure for health
437 care workers. The copy numbers of viral RNA, as estimated by quantifying the nucleocapsid
438 gene region, varied by four orders magnitude suggesting multiple factors including the initial
439 inoculum as a major determinants of viral load in the respiratory tract. Despite this huge
440 variation in viral load, the clinical features and disease outcome did not vary as all patients were
441 able to clear the virus and recover from the disease. This clearly suggests that a robust immune
442 response in younger adults is capable to clearing the infection and age and imbalance in immune
443 response could contribute to severe disease in older individuals and patients with co-morbidities.
444 We observed that decrease in viral loads coincided with increase in IFN responses which is in
445 agreement with observations made by other groups in *ex vivo*, cell culture and animal models
446 where SARS-CoV-2 was shown to be a more potent inhibitor of IFN responses than SARS-CoV-
447 1 (29, 30). Although our study does not have relative comparison between samples from
448 different severities, we observed a consistent decrease in type I and type II during the acute
449 phase of infection. Low serum interferons preceded respiratory failure in critical COVID-19

450 cases (7) whereas we observed an increase in both IFN-α and IFN-γ in all the patients who
451 recovered and were discharged in our study clearly indicating a critical role for interferon
452 responses in recovery from COVID-19. Increase in type I and II interferons indicate activation of
453 T cells and NK cells in addition to the monocytes and macrophages which may contribute to the
454 interferon levels. We have not assessed the levels of IFN-λ in these samples which is known to
455 play a major role in antiviral response from epithelial cells (31). Our results show that there was
456 moderate to no induction of pro-inflammatory cytokines or chemokines such as IL-6, TNF-α, IP-
457 10 in any of these patients. We also observed, at later stages of infection, a trend showing
458 increase in IL-10, IL-4 and IL-1β and IL-12p70 suggesting activation of T cells. Interestingly,
459 IL-8, the primary chemoattractant for neutrophil recruitment has been shown to play an
460 important role in acute respiratory distress syndrome (ARDS) and in recruitment of neutrophils
461 to the site of injury in lungs in sepsis (32). We speculate that generation of high levels of IL-8 by
462 the cells of innate immune system such as macrophages leading to activation of neutrophils
463 which engage in viral clearance from the respiratory tract. Interestingly, neutrophils have been
464 shown to play a crucial antiviral role in influenza A virus infection and in neurotropic
465 coronavirus models such as mouse hepatitis virus (33). However, sustained levels of IL-8 may
466 lead to ARDS observed in severe COVID-19 patients. Therefore, we hypothesize that regulation
467 of IL-8 signalling and neutrophil activity could be an important determinant of clinical outcomes
468 in COVID-19 patients.
469
470 An earlier study from India reported the isolation of SARS-CoV-2 from an Indian patient and its
471 characterization (34). We got one step further and generate the first plaque-purified SARS-CoV-
472 2 isolate from India. Plaque-purified SARS-CoV-2 revealed clear and homogeneous plaques on

473 Vero E6 monolayers compared to the Wuhan strain where the plaques were very heterogeneous
474 in size. As robust and consistent plaque reduction neutralization titers (PRNT) depend on high
475 quality plaque assays, we believe our virus strain will help in establishing PRNT assays that
476 could work reliably and consistently and help vaccine studies. Although SARS-CoV-2 primarily
477 targets the respiratory system, *in vitro* and *in vivo* studies indicate broad tissue tropism (35). In
478 contrast to a previous study which showed no difference between the permissibility of Calu-3
479 and Caco-2 cells for SARS-CoV-2 infection (35), the Indian SARS-CoV-2 isolate from our study
480 infected Calu-3 cells better than Caco-2 cells. Interestingly, cell surface expressions of ACE2 on
481 Caco-2 cells was shown to be higher than Calu-3 cells grown on trans-well inserts (36).
482 Therefore, it would be interesting to investigate the difference in ACE2 expression under
483 different growth conditions and passage history of cell lines to correlate with their susceptibility
484 to infection by SARS-CoV-2. Finally, based on previous reports which demonstrate the
485 inhibitory activity of zinc on coronavirus RNA polymerase (28) and the widely accepted
486 beneficial role of zinc supplementation in respiratory infections (37), we show presence of
487 excess zinc was inhibitory to SARS-CoV-2 in Calu-3 cells. As zinc is an acute-phase reactant
488 which undergoes tissue redistribution during infection, our data suggests a beneficial effect of
489 zinc supplementation in COVID-19 infection.
490

491 **ACKNOWLEDGEMENTS**

492 We thank Amresh Kumar Singh for technical support and all members of CCV lab and bioassay
493 lab for their technical help and critical inputs. We thank all the patients who consented to
494 participate in the study.
495

496 **AUTHOR CONTRIBUTIONS**

497 AA, SG, SK, JW, NAK, AP, NAK, AK, VA, JSV and RP performed experiments and analyzed
498 the data. AD and AKP coordinated the study at clinical site and contributed reagents. GRM
499 conceived the study, designed the experiments, and analyzed data. AA, SG, SK, JW and GRM
500 wrote the manuscript. All authors have reviewed and approved the final version of the
501 manuscript.

502

503 **CONFLICT OF INTEREST STATEMENT**

504 The authors declare that they have no conflict of interest to disclose.

505

506 **FUNDING INFORMATION**

507 This work was supported by funding to GRM by the Biotechnology Industry Research
508 Assistance Council (BIRAC) (BT/NBM0099/02/18). GRM also received funding from the DBT-
509 Wellcome trust India Alliance intermediate fellowship (IA/S/14/1/501291). RP acknowledges
510 funding support from CSIR (MLP-2005), and FondationBotnar (CLP-0031). The funders had no
511 role in study design, data collection and interpretation or the decision to submit the work for
512 publication.

513

514 **REFERENCES**

515 1. Boni MF, Lemey P, Jiang X, Lam TT, Perry BW, Castoe TA, Rambaut A, Robertson DL.
516 2020. Evolutionary origins of the SARS-CoV-2 sarbecovirus lineage responsible for the
517 COVID-19 pandemic. Nat Microbiol doi:10.1038/s41564-020-0771-4.

518 2. Zhou P, Yang XL, Wang XG, Hu B, Zhang L, Zhang W, Si HR, Zhu Y, Li B, Huang CL,
519 Chen HD, Chen J, Luo Y, Guo H, Jiang RD, Liu MQ, Chen Y, Shen XR, Wang X, Zheng
520 XS, Zhao K, Chen QJ, Deng F, Liu LL, Yan B, Zhan FX, Wang YY, Xiao GF, Shi ZL.
521 2020. A pneumonia outbreak associated with a new coronavirus of probable bat origin.
522 Nature 579:270-273.
523 3. Hoffmann M, Kleine-Weber H, Schroeder S, Kruger N, Herrler T, Erichsen S, Schiergens
524 TS, Herrler G, Wu NH, Nitsche A, Muller MA, Drosten C, Pohlmann S. 2020. SARS-
525 CoV-2 Cell Entry Depends on ACE2 and TMPRSS2 and Is Blocked by a Clinically Proven
526 Protease Inhibitor. Cell 181:271-280 e8.
527 4. Wan Y, Shang J, Graham R, Baric RS, Li F. 2020. Receptor Recognition by the Novel
528 Coronavirus from Wuhan: an Analysis Based on Decade-Long Structural Studies of SARS
529 Coronavirus. J Virol 94.
530 5. Tregoning JS, Brown ES, Cheeseman HM, Flight KE, Higham SL, Lemm NM, Pierce BF,
531 Stirling DC, Wang Z, Pollock KM. 2020. Vaccines for COVID-19. Clin Exp Immunol
532 doi:10.1111/cei.13517.
533 6. Heimfarth L, Serafini MR, Martins-Filho PR, Quintans JSS, Quintans-Junior LJ. 2020.
534 Drug repurposing and cytokine management in response to COVID-19: A review. Int
535 Immunopharmacol 88:106947.
536 7. Hadjadj J, Yatim N, Barnabei L, Corneau A, Boussier J, Smith N, Pere H, Charbit B,
537 Bondet V, Chenevier-Gobeaux C, Breillat P, Carlier N, Gauzit R, Morbieu C, Pene F,
538 Marin N, Roche N, Szwebel TA, Merkling SH, Treluyer JM, Veyer D, Mouthon L, Blanc
539 C, Tharaux PL, Rozenberg F, Fischer A, Duffy D, Rieux-Laucat F, Kerneis S, Terrier B.

540 2020. Impaired type I interferon activity and inflammatory responses in severe COVID-19
541 patients. Science 369:718-724.
542 8. Han H, Ma Q, Li C, Liu R, Zhao L, Wang W, Zhang P, Liu X, Gao G, Liu F, Jiang Y,
543 Cheng X, Zhu C, Xia Y. 2020. Profiling serum cytokines in COVID-19 patients reveals
544 IL-6 and IL-10 are disease severity predictors. Emerg Microbes Infect 9:1123-1130.
545 9. Chen G, Wu D, Guo W, Cao Y, Huang D, Wang H, Wang T, Zhang X, Chen H, Yu H,
546 Zhang X, Zhang M, Wu S, Song J, Chen T, Han M, Li S, Luo X, Zhao J, Ning Q. 2020.
547 Clinical and immunological features of severe and moderate coronavirus disease 2019. J
548 Clin Invest 130:2620-2629.
549 10. Pujadas E, Chaudhry F, McBride R, Richter F, Zhao S, Wajnberg A, Nadkarni G,
550 Glicksberg BS, Houldsworth J, Cordon-Cardo C. 2020. SARS-CoV-2 viral load predicts
551 COVID-19 mortality. Lancet Respir Med 8:e70.
552 11. Beigel JH, Tomashek KM, Dodd LE, Mehta AK, Zingman BS, Kalil AC, Hohmann E, Chu
553 HY, Luetkemeyer A, Kline S, Lopez de Castilla D, Finberg RW, Dierberg K, Tapson V,
554 Hsieh L, Patterson TF, Paredes R, Sweeney DA, Short WR, Touloumi G, Lye DC,
555 Ohmagari N, Oh MD, Ruiz-Palacios GM, Benfield T, Fatkenheuer G, Kortepeter MG,
556 Atmar RL, Creech CB, Lundgren J, Babiker AG, Pett S, Neaton JD, Burgess TH, Bonnett
557 T, Green M, Makowski M, Osinusi A, Nayak S, Lane HC, Members A-SG. 2020.
558 Remdesivir for the Treatment of Covid-19 - Final Report. N Engl J Med
559 doi:10.1056/NEJMoa2007764.
560 12. Zhao Z, Li H, Wu X, Zhong Y, Zhang K, Zhang YP, Boerwinkle E, Fu YX. 2004. Moderate
561 mutation rate in the SARS coronavirus genome and its implications. BMC Evol Biol 4:21.

562 13. Forni D, Cagliani R, Clerici M, Sironi M. 2017. Molecular Evolution of Human
563 Coronavirus Genomes. Trends Microbiol 25:35-48.
564 14. Koyama T, Platt D, Parida L. 2020. Variant analysis of SARS-CoV-2 genomes. Bull World
565 Health Organ 98:495-504.
566 15. Zhang X, Tan Y, Ling Y, Lu G, Liu F, Yi Z, Jia X, Wu M, Shi B, Xu S, Chen J, Wang W,
567 Chen B, Jiang L, Yu S, Lu J, Wang J, Xu M, Yuan Z, Zhang Q, Zhang X, Zhao G, Wang
568 S, Chen S, Lu H. 2020. Viral and host factors related to the clinical outcome of COVID-
569 19. Nature 583:437-440.
570 16. Agrawal T, Schu P, Medigeshi GR. 2013. Adaptor protein complexes-1 and 3 are involved
571 at distinct stages of flavivirus life-cycle. Sci Rep 3:1813.
572 17. Kar M, Khan NA, Panwar A, Bais SS, Basak S, Goel R, Sopory S, Medigeshi GR. 2019.
573 Zinc Chelation Specifically Inhibits Early Stages of Dengue Virus Replication by
574 Activation of NF-kappaB and Induction of Antiviral Response in Epithelial Cells. Front
575 Immunol 10:2347.
576 18. Kumar P, Pandey R, Sharma P, Dhar M, A. V, Uppili B, Vashisht H, Wadhwa S, Tyagi N,
577 Fatihi S, Sharma U, Singh P, Lall H, Datta M, Gupta P, Saini N, Tewari A, Nandi B, Kumar
578 D, Bag S, Gahlot D, Rathore S, Jatana N, Jaiswal V, Gogia H, Madan P, Singh S, Singh P,
579 Dash D, Bala M, Kabra S, Singh S, Mukerji M, Thukral L, Faruq M, Agrawal A, Rakshit
580 P. 2020. Integrated genomic view of SARS-CoV-2 in India [version 1; peer review: 2
581 approved]. Wellcome Open Research 5.
582 19. Quick J, Grubaugh ND, Pullan ST, Claro IM, Smith AD, Gangavarapu K, Oliveira G,
583 Robles-Sikisaka R, Rogers TF, Beutler NA, Burton DR, Lewis-Ximenez LL, de Jesus JG,
584 Giovanetti M, Hill SC, Black A, Bedford T, Carroll MW, Nunes M, Alcantara LC, Jr.,

585 Sabino EC, Baylis SA, Faria NR, Loose M, Simpson JT, Pybus OG, Andersen KG, Loman
586 NJ. 2017. Multiplex PCR method for MinION and Illumina sequencing of Zika and other
587 virus genomes directly from clinical samples. Nat Protoc 12:1261-1276.
588 20. Li H. 2018. Minimap2: pairwise alignment for nucleotide sequences. Bioinformatics
589 34:3094-3100.
590 21. Loman NJ, Quick J, Simpson JT. 2015. A complete bacterial genome assembled de novo
591 using only nanopore sequencing data. Nat Methods 12:733-5.
592 22. Edgar RC. 2004. MUSCLE: multiple sequence alignment with high accuracy and high
593 throughput. Nucleic Acids Res 32:1792-7.
594 23. Price MN, Dehal PS, Arkin AP. 2010. FastTree 2--approximately maximum-likelihood
595 trees for large alignments. PLoS One 5:e9490.
596 24. Letunic I, Bork P. 2019. Interactive Tree Of Life (iTOL) v4: recent updates and new
597 developments. Nucleic Acids Res 47:W256-W259.
598 25. Braakhuis HM, He R, Vandebriel RJ, Gremmer ER, Zwart E, Vermeulen JP, Fokkens P,
599 Boere J, Gosens I, Cassee FR. 2020. An Air-liquid Interface Bronchial Epithelial Model
600 for Realistic, Repeated Inhalation Exposure to Airborne Particles for Toxicity Testing. J
601 Vis Exp doi:10.3791/61210.
602 26. Matsuyama S, Nao N, Shirato K, Kawase M, Saito S, Takayama I, Nagata N, Sekizuka T,
603 Katoh H, Kato F, Sakata M, Tahara M, Kutsuna S, Ohmagari N, Kuroda M, Suzuki T,
604 Kageyama T, Takeda M. 2020. Enhanced isolation of SARS-CoV-2 by TMPRSS2-
605 expressing cells. Proc Natl Acad Sci U S A 117:7001-7003.
606 27. Korber B, Fischer WM, Gnanakaran S, Yoon H, Theiler J, Abfalterer W, Hengartner N,
607 Giorgi EE, Bhattacharya T, Foley B, Hastie KM, Parker MD, Partridge DG, Evans CM,

608 Freeman TM, de Silva TI, Sheffield C-GG, McDanal C, Perez LG, Tang H, Moon-Walker
609 A, Whelan SP, LaBranche CC, Saphire EO, Montefiori DC. 2020. Tracking Changes in
610 SARS-CoV-2 Spike: Evidence that D614G Increases Infectivity of the COVID-19 Virus.
611 Cell 182:812-827 e19.
612 28. te Velthuis AJ, van den Worm SH, Sims AC, Baric RS, Snijder EJ, van Hemert MJ. 2010.
613 Zn(2+) inhibits coronavirus and arterivirus RNA polymerase activity in vitro and zinc
614 ionophores block the replication of these viruses in cell culture. PLoS Pathog 6:e1001176.
615 29. Chu H, Chan JF, Wang Y, Yuen TT, Chai Y, Hou Y, Shuai H, Yang D, Hu B, Huang X,
616 Zhang X, Cai JP, Zhou J, Yuan S, Kok KH, To KK, Chan IH, Zhang AJ, Sit KY, Au WK,
617 Yuen KY. 2020. Comparative Replication and Immune Activation Profiles of SARS-CoV-
618 2 and SARS-CoV in Human Lungs: An Ex Vivo Study With Implications for the
619 Pathogenesis of COVID-19. Clin Infect Dis 71:1400-1409.
620 30. Blanco-Melo D, Nilsson-Payant BE, Liu WC, Uhl S, Hoagland D, Moller R, Jordan TX,
621 Oishi K, Panis M, Sachs D, Wang TT, Schwartz RE, Lim JK, Albrecht RA, tenOever BR.
622 2020. Imbalanced Host Response to SARS-CoV-2 Drives Development of COVID-19.
623 Cell 181:1036-1045 e9.
624 31. Felgenhauer U, Schoen A, Gad HH, Hartmann R, Schaubmar AR, Failing K, Drosten C,
625 Weber F. 2020. Inhibition of SARS-CoV-2 by type I and type III interferons. J Biol Chem
626 295:13958-13964.
627 32. Groeneveld ABJ. A Central Role of Interleukin-8 in the Pathogenesis of ARDS, p 65-74.
628 *In* (ed), Springer Berlin Heidelberg,
629 33. Galani IE, Andreakos E. 2015. Neutrophils in viral infections: Current concepts and
630 caveats. J Leukoc Biol 98:557-64.

631 34. Sarkale P, Patil S, Yadav PD, Nyayanit DA, Sapkal G, Baradkar S, Lakra R, Shete-Aich
632 A, Prasad S, Basu A, Dar L, Vipat V, Giri S, Potdar V, Choudhary ML, Praharaj I, Jain A,
633 Malhotra B, Gawande P, Kalele K, Gupta N, Cherian SS, Abraham P. 2020. First isolation
634 of SARS-CoV-2 from clinical samples in India. Indian J Med Res 151:244-250.
635 35. Chu H, Chan JF, Yuen TT, Shuai H, Yuan S, Wang Y, Hu B, Yip CC, Tsang JO, Huang
636 X, Chai Y, Yang D, Hou Y, Chik KK, Zhang X, Fung AY, Tsoi HW, Cai JP, Chan WM,
637 Ip JD, Chu AW, Zhou J, Lung DC, Kok KH, To KK, Tsang OT, Chan KH, Yuen KY.
638 2020. Comparative tropism, replication kinetics, and cell damage profiling of SARS-CoV-
639 2 and SARS-CoV with implications for clinical manifestations, transmissibility, and
640 laboratory studies of COVID-19: an observational study. Lancet Microbe 1:e14-e23.
641 36. Ren X, Glende J, Al-Falah M, de Vries V, Schwegmann-Wessels C, Qu X, Tan L,
642 Tschernig T, Deng H, Naim HY, Herrler G. 2006. Analysis of ACE2 in polarized epithelial
643 cells: surface expression and function as receptor for severe acute respiratory syndrome-
644 associated coronavirus. J Gen Virol 87:1691-5.
645 37. Lassi ZS, Moin A, Bhutta ZA. 2016. Zinc supplementation for the prevention of pneumonia
646 in children aged 2 months to 59 months. Cochrane Database Syst Rev 12:CD005978.

647

648 **SUPPLEMENTARY INFORMATION**

649 This article has supplementary information.

650

651

652 **TABLE**

653 **Table – 1 List of mutations in plaque-purified isolates compared to the reference Wuhan**

654 **strain (MN908947.3).**

Virus	Nucleotide position	Base change	Open reading frame	Amino acid substitution
THSTI-2010-(A, B, C, D)	1227	T→C	ORF1a	M321T
	1281	C→T	ORF1a	A339V
	1758	C→T	ORF1a	A498V
	4885	T→C	ORF1a	Synonymous
	6312	C→A	ORF1a	T2016K
	11083	G→T	ORF1a	L3606F
	13730	C→T	ORF1b	A88V
	23929	C→T	Surface glycoprotein (S; Spike)	Synonymous
	28311	C→T	Nucleocapsid phosphoprotein (N)	P13L
THSTI-2010-C	27806	G→T	ORF7b	Synonymous

655

656 **FIGURE LEGENDS**

657 **Figure 1: Kinetics of viral load in VTM and saliva samples of COVID-19 patients.** A-F)

658 SARS-CoV-2 RNA levels were measured by RT-PCR using total RNA isolated from VTM

659 samples every day after enrolment. G-K) SARS-CoV-2 RNA levels were measured by RT-PCR
660 using total RNA isolated from saliva and VTM samples every day after enrolment. Data points
661 indicate geometric mean normalized to RNASe P levels which was used as endogenous controls
662 for extraction efficiency.
663
664 **Figure 2: Kinetics of secreted inflammatory mediators in COVID-19 patients.** A) Daily
665 IFN-α, IFN-γ levels (on the left y-axis) were estimated from serum samples of COVID-19
666 patients using luminex assays and copy numbers of viral genome equivalents (on the right-y
667 axis) was estimated from RNA isolated from VTM samples every day. B) The levels of indicated
668 cytokines influencing T-cell functions were estimated from serum samples collected daily from
669 COVID-19 patients. C) The levels of indicated chemokines suggestive of inflammation were
670 estimated from serum samples collected daily from COVID-19 patients. D) The levels of
671 indicated cytokines which are key determinants of inflammatory response were estimated from
672 serum samples collected daily from COVID-19 patients. Columns indicate the median value with
673 95% CI.
674
675 **Figure 3: THSTI-BL-2010 plaque-purified isolates.** A) Single plaque morphology of THSTI-
676 BL-2010 at 72 h pi. Virus from four single plaques were propagated on VeroE6 monolayer
677 separately. Cytopathic effect was evident at 72 h post-infection for all the four isolates. Images
678 were captured at 20X magnification. B) VeroE6 cells were used for performing plaque assays
679 with either the reference SARS-CoV-2 strain or THSTI-BL-2010D.Cells were fixed at 60 h pi
680 and stained with crystal violet.
681

682 **Figure 4: Infection of human cell lines.** A) Vero E6, Calu-3 and Caco-2 cells were either
683 mock-infected or infected with THSTI-2010-D at indicated MOI for 24 h. Cells were fixed in
684 and stained with anti-spike protein antibody and probed with secondary antibody conjugated
685 with Alexa Fluor 488. Images were captured using Olympus DP80 microscope. Scale bar is 100
686 µm. B) Growth curve of SARS-CoV-2 Wuhan and THSTI-BL2010D strain were compared on
687 Vero E6 cells. Vero E6 cells were infected at 0.1 MOI either with Wuhan strain or THSTI
688 BL2010D. Viral titers were measured at 24 h, 48 h and 72 h in culture supernatants (n=3).
689
690 **Figure 5. Maximum likelihood phylogeny for SARS CoV2 sequences (n=100).** Indian isolates
691 reported here falls under 19A clade. The sequence of plaque purified isolates are highlighted
692 with symbol 'star'. The GISAID clades are indicated as mentioned in the inset. The scale bar
693 indicates the branch lengths measured in number of nucleotide substitution rate per site.
694
695 **Figure 6: SARS-CoV-2 infection disrupts epithelial barrier integrity.** A) Calu-3 cells grown
696 on transwells at air-liquid interface as described in methods section. Polarized Calu-3 cells were
697 infected with SARS-CoV-2 THSTI-BL-2010D at 0.3 MOI. TEER was measured at 24 h pi.
698 TEER values were represented as ohm/cm^2. B) Viral titres were determined at 24 h pi and
699 represented as pfu/ml. C) Cells were fixed and stained with ZO-1 and Claudin-3 antibodies
700 against cellular junctions and spike antibody against viral protein. Nuclei were stained with
701 DAPI. Images were captured at 100X. Representative images of mock and SARS-CoV-2
702 infected cells are displayed. Scale bar is 10 µm. D) Calu-3 cells were treated with indicated
703 concentrations of $ZnSO_4$ for 24 h and cell viability was measured using CellTiter-Glo® Assay
704 kit. E) Calu-3 cells were infected with SARS-CoV-2-THSTI-BL-2010D at 0.3 MOI. After viral

705 adsorption, cells were treated with 25 and 50 μM of $ZnSO_4$ or as mock treated control. Viral
706 titres were determined as represented as pfu/ml. (n=3). Error bars represent mean ± SD. *p <
707 0.05, **p < 0.01.
708
709
710 **SUPPLEMENTARY FIGURE LEGENDS**
711 **Figure S1: SARS-CoV-2 Indian isolates.** Vero E6 cells were infected with nasopharyngeal
712 swab samples for 1 h and cultured in growth medium thereafter. CPE was evident at 48 h post-
713 infection. Images were captured using Nikon Eclipse Ti-S microscope at 20X magnification.
714
715 **Figure S2: Zinc uptake in Calu-3 cells.** Calu-3 cells after incubation with indicated
716 concentrations of zinc sulfate for 4 h and labile zinc levels were measured by staining with
717 ZinPyr-1 and flow cytometry. The relative change in the mean fluorescence intensities of ZP-1 is
718 shown in the graph. Error bars represent Mean with SD.
719
720
721

Figure 1

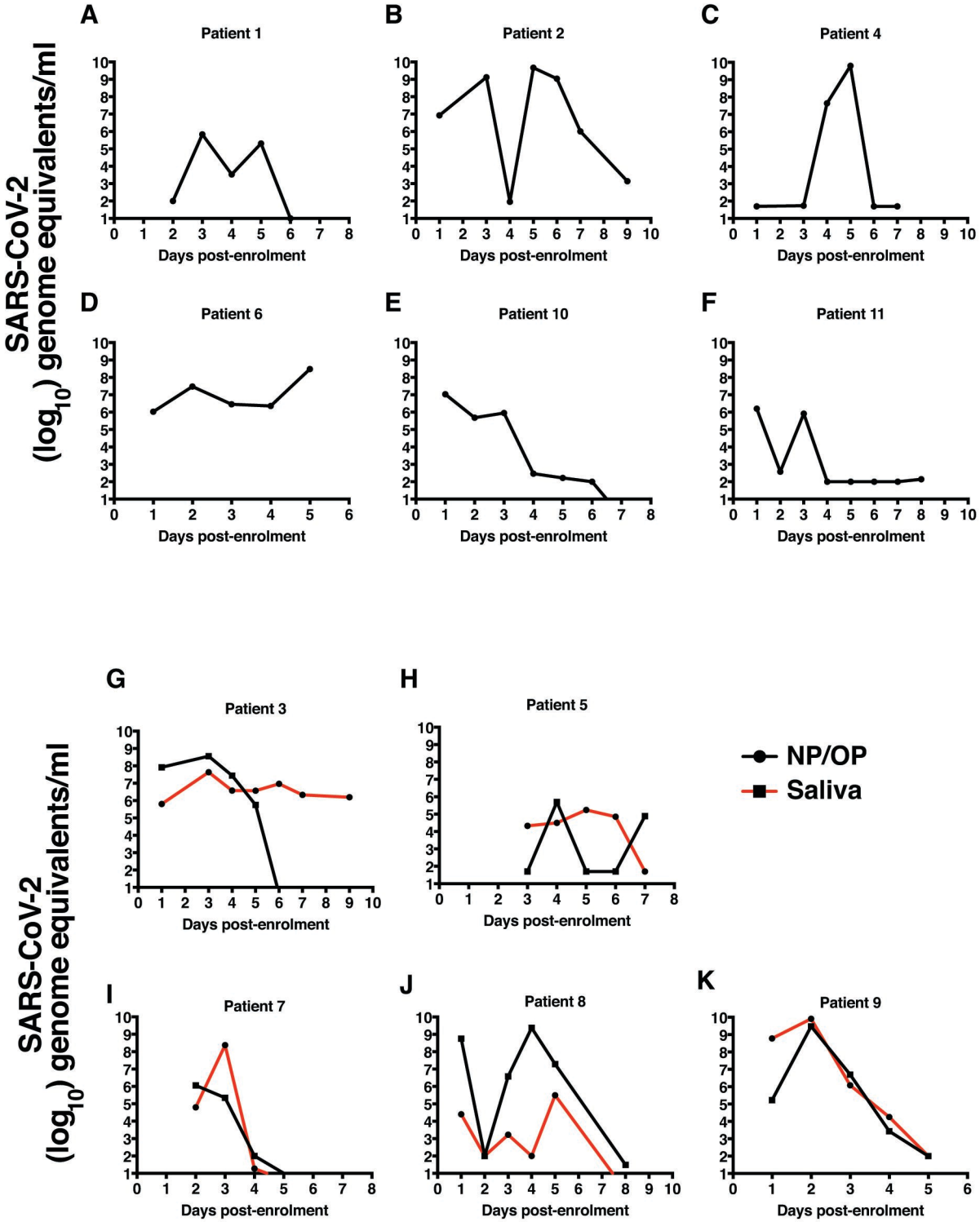
A
Patient 1
B
Patient 2
C
Patient 4
D
Patient 6
E
Patient 10
F
Patient 11
G
Patient 3
H
Patient 5
I
Patient 7
J
Patient 8
K
Patient 9
SARS-CoV-2 (log10) genome equivalents/ml
Days post-enrolment
NP/OP
Saliva

Figure 2

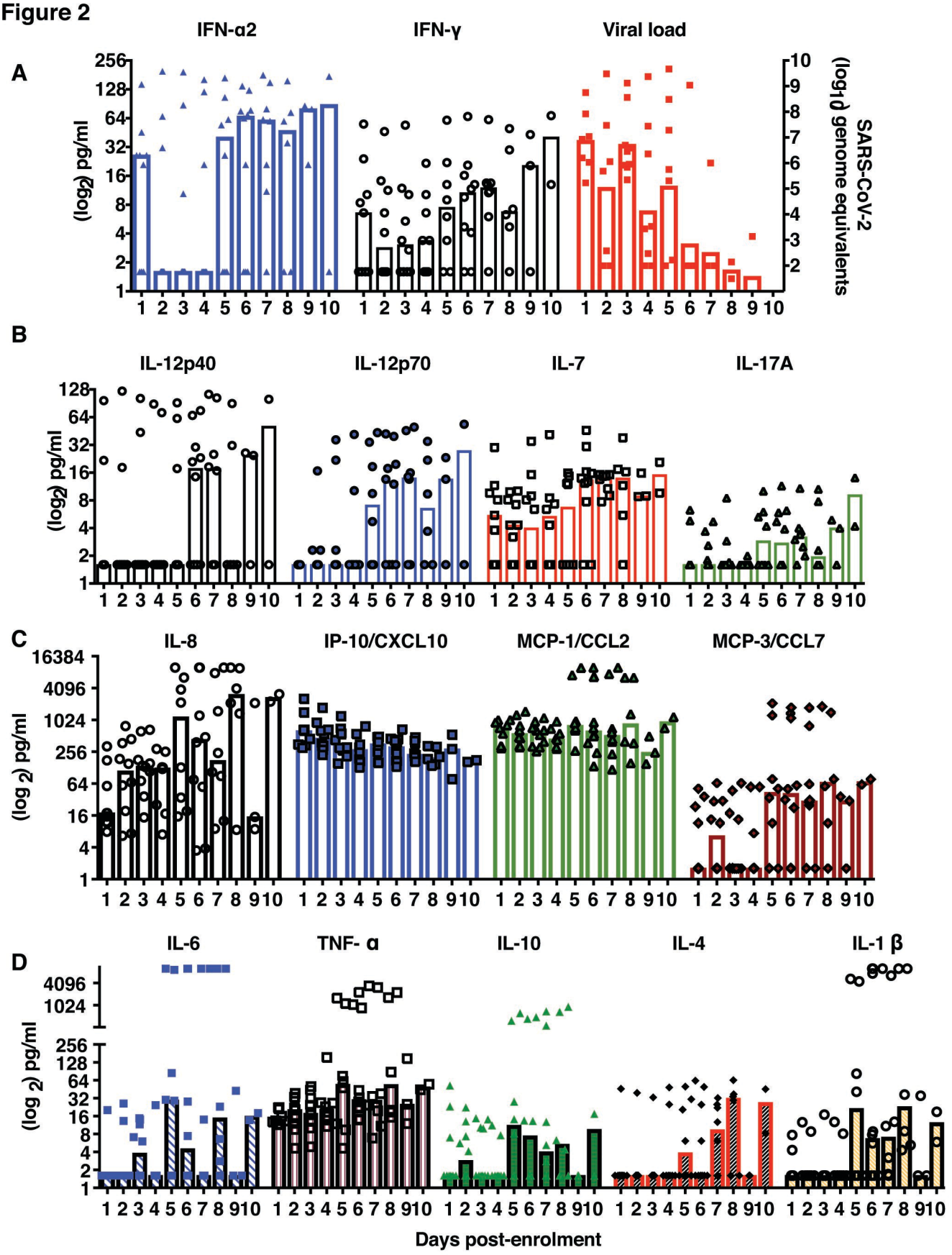
A
IFN-α2
IFN-γ
Viral load
(log2) pg/ml
(log10) genome equivalents
SARS-CoV-2
B
IL-12p40
IL-12p70
IL-7
IL-17A
(log2) pg/ml
C
IL-8
IP-10/CXCL10
MCP-1/CCL2
MCP-3/CCL7
(log 2) pg/ml
D
IL-6
TNF- α
IL-10
IL-4
IL-1 β
(log 2) pg/ml
Days post-enrolment

Figure 3

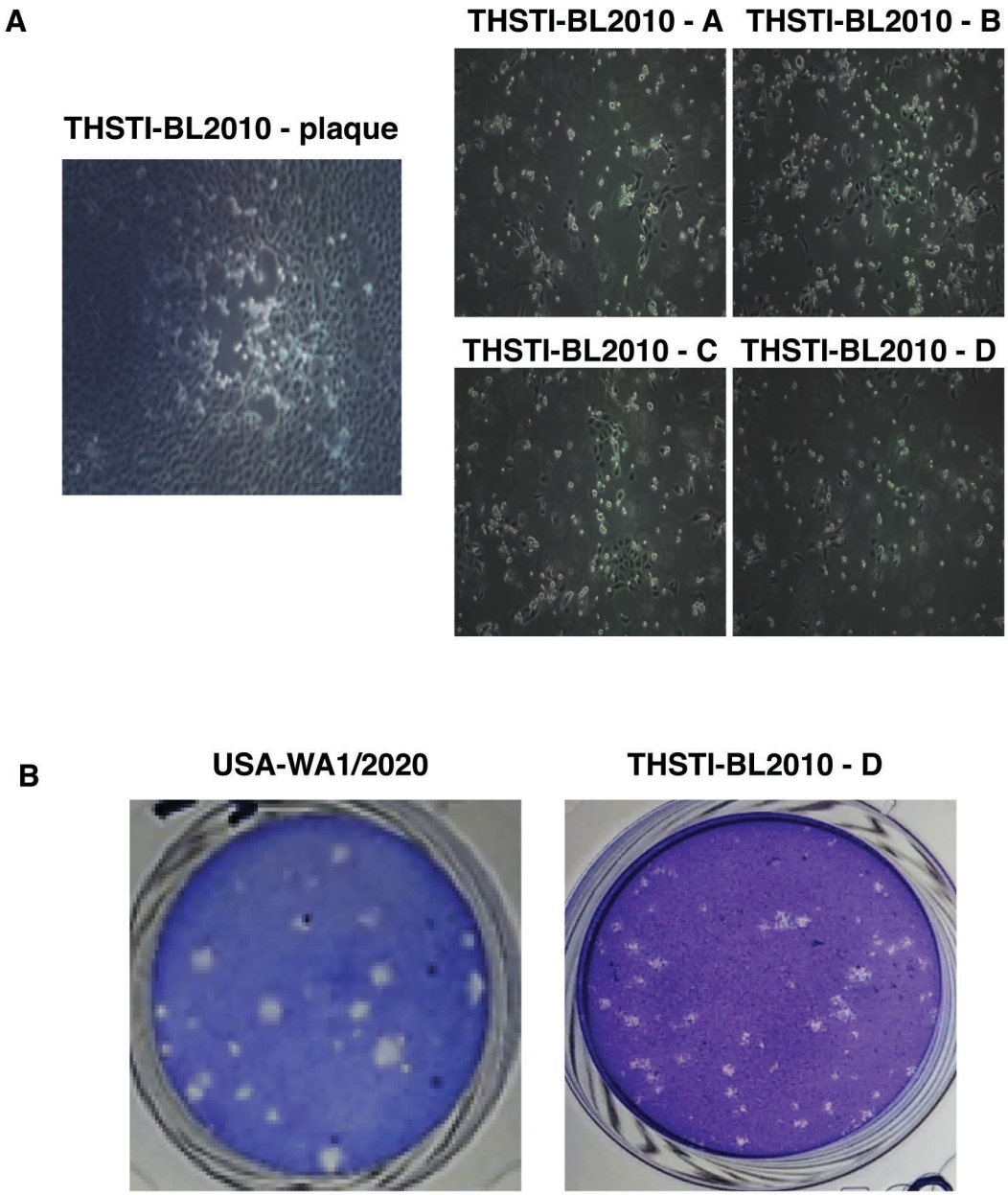
A
THSTI-BL2010 - plaque
THSTI-BL2010 - A
THSTI-BL2010 - B
THSTI-BL2010 - C
THSTI-BL2010 - D
B
USA-WA1/2020
THSTI-BL2010 - D

Figure 4

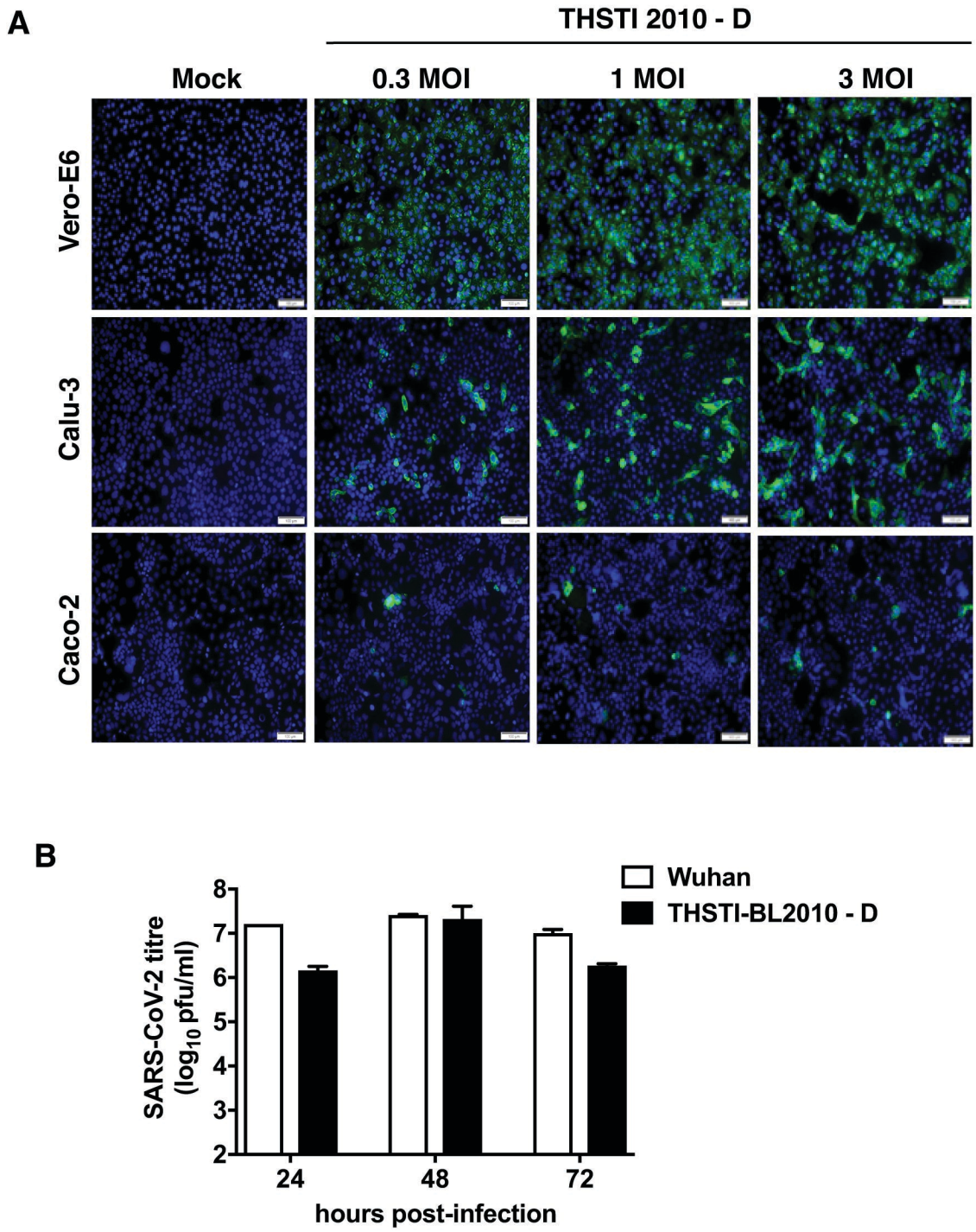
A
THSTI 2010 - D
Mock
0.3 MOI
1 MOI
3 MOI
Vero-E6
Calu-3
Caco-2
B
Wuhan
THSTI-BL2010 - D
SARS-CoV-2 titre
(log10 pfu/ml)
8
7
6
5
4
3
2
24
48
72
hours post-infection

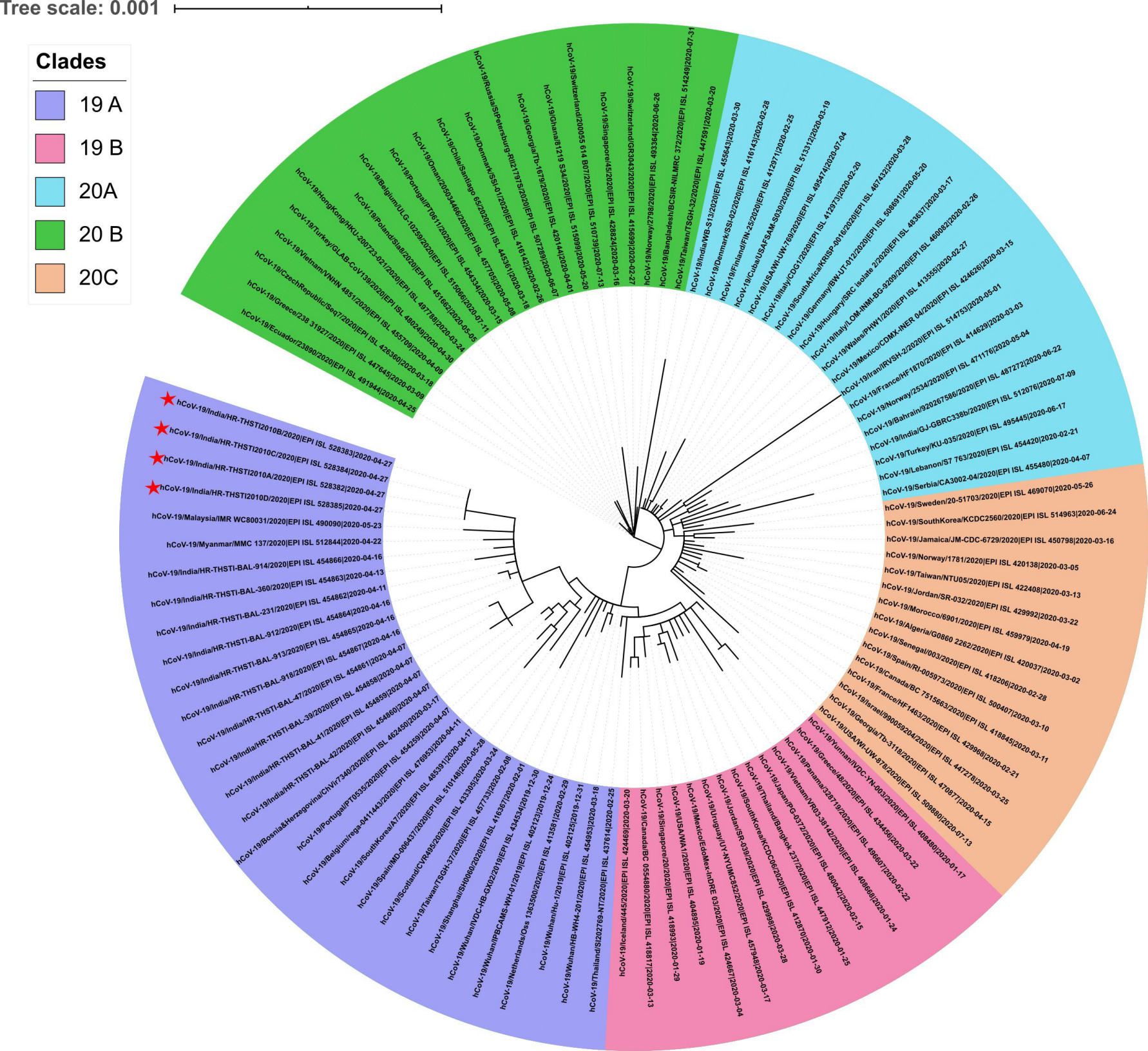
Tree scale: 0.001
Clades
19 A
19 B
20A
20 B
20C
hCoV-19/India/HR-THSTI2010B/2020|EPI ISL 528383|2020-04-27
hCoV-19/India/HR-THSTI2010C/2020|EPI ISL 528384|2020-04-27
hCoV-19/India/HR-THSTI2010A/2020|EPI ISL 528382|2020-04-27
hCoV-19/India/HR-THSTI2010D/2020|EPI ISL 528385|2020-04-27
hCoV-19/Malaysia/IMR WC80031/2020|EPI ISL 490090|2020-05-23
hCoV-19/Myanmar/MMC 137/2020|EPI ISL 512844|2020-04-22
hCoV-19/India/HR-THSTI-BAL-914/2020|EPI ISL 454866|2020-04-16
hCoV-19/India/HR-THSTI-BAL-360/2020|EPI ISL 454863|2020-04-13
hCoV-19/India/HR-THSTI-BAL-231/2020|EPI ISL 454862|2020-04-11
hCoV-19/India/HR-THSTI-BAL-912/2020|EPI ISL 454864|2020-04-16
hCoV-19/India/HR-THSTI-BAL-913/2020|EPI ISL 454865|2020-04-16
hCoV-19/India/HR-THSTI-BAL-918/2020|EPI ISL 454867|2020-04-16
hCoV-19/India/HR-THSTI-BAL-47/2020|EPI ISL 454861|2020-04-07
hCoV-19/India/HR-THSTI-BAL-39/2020|EPI ISL 454858|2020-04-07
hCoV-19/India/HR-THSTI-BAL-41/2020|EPI ISL 454859|2020-04-07
hCoV-19/India/HR-THSTI-BAL-42/2020|EPI ISL 454860|2020-04-07
hCoV-19/Bosnia&Herzegovina/ChVir7340/2020|EPI ISL 462450|2020-03-17
hCoV-19/Portugal/PT0535/2020|EPI ISL 454259|2020-04-11
hCoV-19/Belgium/rega-0411443/2020|EPI ISL 476959|2020-04-17
hCoV-19/SouthKorea/A7/2020|EPI ISL 485391|2020-04-17
hCoV-19/Spain/MD-006437/2020|EPI ISL 510148|2020-05-28
hCoV-19/Scotland/CVR495/2020|EPI ISL 433305|2020-03-24
hCoV-19/Taiwan/TSGH-37/2020|EPI ISL 457733|2020-02-08
hCoV-19/Shanghai/SH0060/2020|EPI ISL 416367|2020-02-01
hCoV-19/Wuhan/IVDC-HB-GX02/2019|EPI ISL 434534|2019-12-30
hCoV-19/Wuhan/IPBCAMS-WH-01/2019|EPI ISL 402123|2019-12-24
hCoV-19/Netherlands/Oss 1363500/2020|EPI ISL 413881|2020-02-29
hCoV-19/Wuhan/Hu-1/2019|EPI ISL 402125|2019-12-31
hCoV-19/Wuhan/HB-WH4-201/2020|EPI ISL 454953|2020-03-18
hCoV-19/Thailand/SI202769-NT/2020|EPI ISL 437614|2020-02-25
hCoV-19/Iceland/445/2020|EPI ISL 424469|2020-03-20
hCoV-19/Canada/BC 0554880/2020|EPI ISL 418817|2020-03-13
hCoV-19/Singapore/20/2020|EPI ISL 418993|2020-01-29
hCoV-19/USA/WA1/2020|EPI ISL 404895|2020-01-19
hCoV-19/Mexico/EdoMex-InDRE 03/2020|EPI ISL 424667|2020-03-04
hCoV-19/Uruguay/UY-NYUMC852/2020|EPI ISL 457948|2020-03-17
hCoV-19/Jordan/SR-039/2020|EPI ISL 429999|2020-03-28
hCoV-19/SouthKorea/KCDC06/2020|EPI ISL 412870|2020-01-30
hCoV-19/Thailand/Bangkok-237/2020|EPI ISL 447912|2020-01-25
hCoV-19/Japan/PG-0372/2020|EPI ISL 480042|2020-02-15
hCoV-19/Vietnam/VR03-381/2020|EPI ISL 408668|2020-01-24
hCoV-19/Panama/328719/2020|EPI ISL 496607|2020-02-22
hCoV-19/Greece/48/2020|EPI ISL 434456|2020-03-22
hCoV-19/Yunnan/IVDC-YN-003/2020|EPI ISL 408480|2020-01-17
hCoV-19/USA/WI-UW-879/2020|EPI ISL 509980|2020-07-13
hCoV-19/Georgia/Tb-3118/2020|EPI ISL 470877|2020-04-15
hCoV-19/Israel/990059204/2020|EPI ISL 447278|2020-03-25
hCoV-19/France/HF1463/2020|EPI ISL 429968|2020-02-21
hCoV-19/Canada/BC 7515663/2020|EPI ISL 418845|2020-03-11
hCoV-19/Spain/RI-005973/2020|EPI ISL 500407|2020-03-10
hCoV-19/Senegal/003/2020|EPI ISL 418206|2020-02-28
hCoV-19/Algeria/G0860 2262/2020|EPI ISL 420037|2020-03-02
hCoV-19/Morocco/6901/2020|EPI ISL 459979|2020-04-19
hCoV-19/Jordan/SR-032/2020|EPI ISL 429992|2020-03-22
hCoV-19/Taiwan/NTU05/2020|EPI ISL 422408|2020-03-13
hCoV-19/Norway/1781/2020|EPI ISL 420138|2020-03-05
hCoV-19/Jamaica/JM-CDC-6729/2020|EPI ISL 450798|2020-03-16
hCoV-19/SouthKorea/KCDC2560/2020|EPI ISL 514963|2020-06-24
hCoV-19/Sweden/20-51703/2020|EPI ISL 469070|2020-05-26
hCoV-19/Serbia/CA3002-04/2020|EPI ISL 455480|2020-04-07
hCoV-19/Lebanon/S7 763/2020|EPI ISL 454420|2020-02-21
hCoV-19/Turkey/KU-035/2020|EPI ISL 495445|2020-06-17
hCoV-19/India/GJ-GBRC338b/2020|EPI ISL 512076|2020-07-09
hCoV-19/Bahrain/920267586/2020|EPI ISL 487272|2020-06-22
hCoV-19/Norway/2534/2020|EPI ISL 471176|2020-05-04
hCoV-19/France/HF1870/2020|EPI ISL 414629|2020-03-03
hCoV-19/Iran/IRVSH-2/2020|EPI ISL 514753|2020-05-01
hCoV-19/Mexico/CDMX-INER 04/2020|EPI ISL 424626|2020-03-15
hCoV-19/Wales/PHW12020|EPI ISL 413555|2020-02-27
hCoV-19/Italy/LOM-INMI-BG-9209/2020|EPI ISL 460082|2020-02-26
hCoV-19/Hungary/SRC isolate 2/2020|EPI ISL 483637|2020-03-17
hCoV-19/Germany/BW-UT-012/2020|EPI ISL 508691|2020-05-20
hCoV-19/SouthAfrica/KRISP-0016/2020|EPI ISL 467432|2020-03-28
hCoV-19/Italy/CDG1/2020|EPI ISL 412973|2020-02-20
hCoV-19/USA/NY-UW-769/2020|EPI ISL 495474|2020-07-04
hCoV-19/Cuba/USAFSAM-S030/2020|EPI ISL 513312|2020-03-19
hCoV-19/Finland/FIN-25/2020|EPI ISL 412971|2020-02-25
hCoV-19/Denmark/SSI-02/2020|EPI ISL 416143|2020-02-28
hCoV-19/India/WB-S13/2020|EPI ISL 455643|2020-03-30
hCoV-19/Taiwan/TSGH-32/2020|EPI ISL 447591|2020-03-20
hCoV-19/Bangladesh/BCSIR-NILMRC 372/2020|EPI ISL 514249|2020-07-31
hCoV-19/Norway/2798/2020|EPI ISL 493364|2020-06-26
hCoV-19/Switzerland/GR3043/2020|EPI ISL 415699|2020-02-27
hCoV-19/Singapore/45/2020|EPI ISL 428824|2020-03-16
hCoV-19/Switzerland/200055 614 B07/2020|EPI ISL 510739|2020-07-13
hCoV-19/Ghana/81219 S34/2020|EPI ISL 420144|2020-04-01
hCoV-19/Georgia/Tb-1679/2020|EPI ISL 507289|2020-06-07
hCoV-19/Russia/StPetersburg-RII21797S/2020|EPI ISL 416142|2020-02-26
hCoV-19/Denmark/SSI-01/2020|EPI ISL 445361|2020-03-18
hCoV-19/Chile/Santiago 65/2020|EPI ISL 457705|2020-05-08
hCoV-19/Oman/2050344662020|EPI ISL 454334|2020-03-15
hCoV-19/Portugal/PT0611/2020|EPI ISL 451662|2020-07-11
hCoV-19/Belgium/ULG-10259/2020|EPI ISL 515068|2020-05-05
hCoV-19/Poland/Sla8/2020|EPI ISL 497788|2020-03-24
hCoV-19/HongKong/HKU-200723-021/2020|EPI ISL 480249|2020-04-30
hCoV-19/Turkey/GLAB-CoV139/2020|EPI ISL 455709|2020-04-09
hCoV-19/Vietnam/VNHN 4851/2020|EPI ISL 426360|2020-03-18
hCoV-19/CzechRepublic/Seq7/2020|EPI ISL 447645|2020-03-09
hCoV-19/Greece/238 31927/2020|EPI ISL 491944|2020-04-25
hCoV-19/Ecuador/23890/2020|EPI ISL 447645|2020-03-09

Figure 6

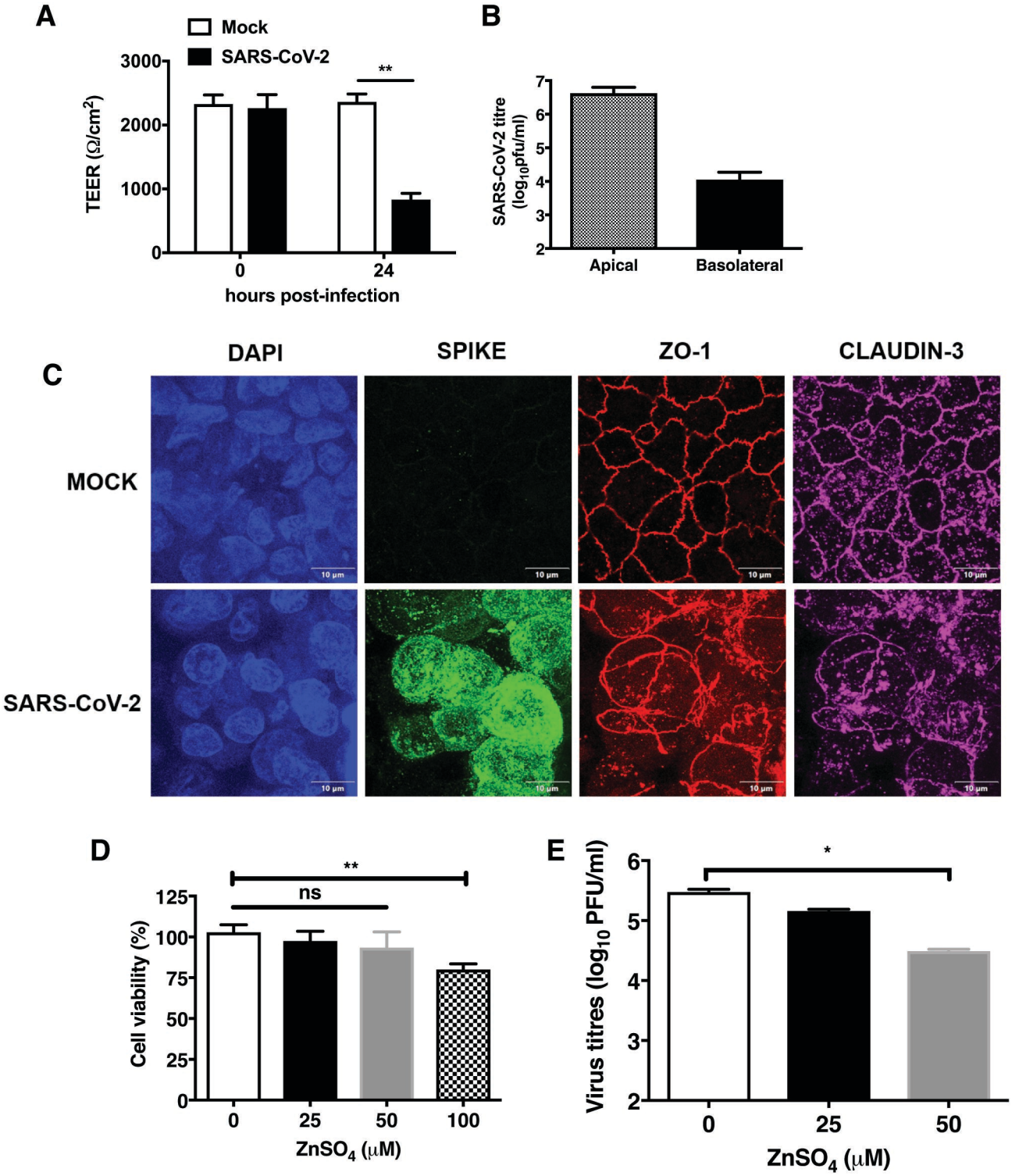
A
Mock
SARS-CoV-2
**
TEER (Ω/cm²)
3000
2000
1000
0
0
24
hours post-infection
B
SARS-CoV-2 titre (log10pfu/ml)
7
6
5
4
3
2
Apical
Basolateral
C
DAPI
SPIKE
ZO-1
CLAUDIN-3
MOCK
SARS-CoV-2
10 µm
D
**
ns
Cell viability (%)
125
100
75
50
25
0
0
25
50
100
ZnSO4 (µM)
E
*
Virus titres (log10 PFU/ml)
6
5
4
3
2
0
25
50
ZnSO4 (µM)